Pufferfish Optimization based MPPT of PV System under Partial Shading Conditions for SRM Driven Water Pumping Applications

Sushil Kumar Bhoi[1*], Jayanta Kumar Panigrahi[2] and Bikash Meher[3]

[1]Department of Electrical Engineering, Government College of Engineering Kalahandi, Bhawanipatna , Odisha,India, PIN- 766003

[1*]sushilkumarbhoi@gmail.com, [2]jayanta.panigrahi@gmail.com, [3]bikashmeher1981@gmail.com,

Abstract: Water Pumping Systems (WPSs) are mandatory components in numerous facets of human existence, encompassing drinking water supply, agricultural activities, and industrial applications. In numerous places, a locally installed standby Photovoltaic (PV) powered WPS is regarded as the most feasible option for water supply. In some instances, it is necessary to utilize several WPS units to satisfy the demand. This study examines the analysis of two WPSs that are supplied by a shared PV system and a common converter. An electric motor is essential for extracting water from subterranean sources. Among the different types of motors available, switched reluctance motors (SRMs) stand out as particularly appealing for WPSs because of their numerous benefits. To eliminate the expenses and upkeep linked to batteries, this paper explores a PV-powered switched reluctance motor (SRM) utilized in a WPS that operates without a battery bank. A sensorless speed controller utilizing a sliding mode controller (SMC) is employed to control the speed of the SRM without the necessity of sensors for obtains speed of the motors. Partial shading frequently occurs in PV systems and can significantly affect power generation. The Perturbed and Observe (P&O) methodology by itself is inadequate for generating a voltage signal that aligns with the maximum power point (MPP) in the operation under Partial Shading Conditions (PSCs). Consequently, the Pufferfish algorithm is adding with the P&O method to function efficiently in the context of PSCs. The outcomes of this integration are evaluated against PSO, GA, and MGWO for Maximum Power Point Tracking (MPPT) under various PSCs. By combining the proposed MPPT methodology with SMC, the converter is capable of operating as an MPPT device. Comprehensive testing and validation of the proposed system are performed on the OPAL-RT platform.

Keywords: Water Pumping, MPPT, Partial Shading, PV, SRM, Sliding Mode, MRAC, Pufferfish Optimization Algorithm.

I. INTRODUCTION

Water is an essential requirement for human existence. The delivery of water via pumps is fundamental to numerous sectors, including industries, agriculture and drinking uses. The efficiency of agricultural operations is significantly dependent on water resources, a concern that becomes increasingly critical during the summer months due to limited water resources. In addition to agricultural uses, water is essential for human consumption, and industries depend on a steady supply of water to fulfill their requirements. WPS generally require a considerable amount of energy or electrical power to meet these demands. During the summer months, we are presented with the opportunity to capture significant solar energy and transform it into electrical power through the application of PV technology [1].

Solar-powered pumps represent an environmentally advantageous solution, as they contribute to the reduction of carbon dioxide emissions and function with minimal noise [2-3]. Solar water pumps are gaining popularity, particularly in rural and remote regions, as they do not depend on electrical motors or diesel generators, which are often hindered by an unreliable power supply. Diesel generators are not only costly but also detrimental to the environment. Furthermore, supplying electricity to rural regions is frequently unfeasible in numerous areas across the globe. Implementing solar-powered pumps in conjunction with locally installed PV systems presents a financially viable and environmentally sustainable alternative to conventional pumping methods.

The adoption of PV-based WPSs has seen a significant increase in numerous countries in recent times. These systems, which operate without the need for batteries, provide a cost-efficient and maintenance-free alternative [4]. Nevertheless, extensive agricultural areas require several WPSs to guarantee a sufficient water supply. The presence of distinct converters for each system elevates the total cost of the overall model. In order to tackle this issue, a unified converter-PV system is suggested, which utilizes two identical SRMs to operate two WPSs. Generally SRMs are more suitable for WPS applications [5]. In conditions of low irradiance, only one pump is operating with a motor, whereas the second one functions concurrently when the PV system provides adequate power. Consequently, a shared PV system is employed to supply energy to both SRMs. To obtain a better efficiency of PV modules, it is essential to employ a MPPT device equipped with a suitable algorithm to extract the possible high energy from the PV modules. The incorporation of this device results in an increase in both the total cost and size [6]. Therefore, single-stage PV-powered WPSs can be a cost-effective solution while maintaining a compact design [6-7]. Numerous researchers have suggested PV-based WPSs utilizing different types of AC motors; however, SRMs are regarded as the most appropriate choice for such systems [5]. Numerous algorithms exist for identifying the MPP, yet the P&O algorithm stands out to researchers because of its straightforwardness and remarkable efficiency [2-3, 8]. A PV unit generally comprises several PV modules arranged in both series and parallel configurations, with each module containing numerous PV cells. Consequently, the PV system may experience partial shading due to various factors, including dust, trees, buildings, birds, and clouds [6, 9-10]. The traditional P&O approach fails to effectively track the MPP

in the presence of PSC because of the presence of several local maximum power locations (LM) [9]. To effectively track the global maximum power location (GM), it's crucial to combine an optimization technique with the P&O methodology. Many researchers have proposed MPPT methods for PV-based WPS, as highlighted below. In [5], the authors developed a WPS driven by a synchronous reluctance motor supplied by PV under PSCs.

Among various optimization techniques, the Pufferfish Optimization Algorithm (POA) is distinguished as a widely recognized approach capable of effectively identifying the GM point [11]. This document presents the hybrid POA - P&O (POPO) algorithm, designed for monitoring the MPP level in the context of PSCs. In order to achieve a better system's performance in the context of PSCs, the proposed POPO algorithm is evaluated against three established methods: GA-Genetic Algorithm [14], PSO-Particle Swarm Optimization [15], and MGWO-Modified Grey Wolf Optimization [5].

An appropriate converter controller is essential for the efficient functioning of the 8/6 pole SRMs. The installation of a speed sensor for measurement presents difficulties and costs, primarily because the motor-pump assembly is located underwater. Consequently, this document advocates for the adoption of a speed sensorless controller. A SMC is utilized to adjust the motor's speed in alignment with the power availability of the PV system. The motor's speed is regulated by adjusting the dc-link voltage of the converter to match its reference value, which is generated by POPO, as demonstrated in Figure 1 in the DC-link control (DCLC) section. The Takagi-Sugeno Fuzzy (TS-Fuzzy) controller demonstrates superior effectiveness in managing the motor's speed during swift changes in irradiance when compared to the PI controller [16]. Consequently, a TS-Fuzzy based controller has been employed to adjust the speed of the SRM(s).

II. System Description

The depicted WPS in Figure 1 consists of a PV unit designed to provide electrical energy, a singular converter, two SRMs, and a novel converter controller. Given that submersible pumps are employed, the motors will likewise be immersed in water. Consequently, it becomes challenging to gauge the speed of the motors during their operation. In order to address this challenge, a sensorless speed control (SSC) has been established through the application of mathematical formulas, and a SMC has been designed to manage the dc-link voltage by producing a reference sped signal for the SRMs. The elements have been carefully crafted and designed, with the specifics outlined below.

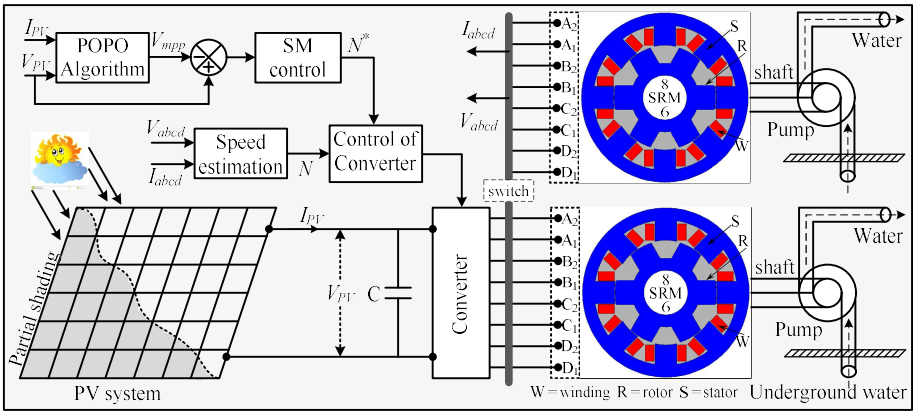

Figure 1: PV fed WPS driven by multiple SRMs.

a. Water Pumps [5, 9]

Generally, the breakaway torque (Tb) for a motor or pump is expected to be around 5% to 30% of the general torque. This torque is essential to surpass the static friction present in the running components that are engaged in the process of lifting the water. When the pump's speed attains a specific baseline point (ω_t), it commences the delivery of water. The motor speed decided the flow rate of water (Q, gal/min) as demonstrated by eq. (1) [9]. Furthermore, the governing dynamics of the system's head are described by a nonlinear equation, as illustrated in equation (2).

$$Q = \begin{cases} x_1\omega - x_2 & \omega \geq \omega_t \\ 0 & \omega < \omega_t \end{cases} \quad (1)$$

$$H = x_3\omega^2 + x_4\omega Q + x_5 Q^2 \quad (2)$$

The process entails assessing the necessary horsepower capacity for an individual motor.

$$W_{hp} = \frac{Q \times H}{3960} \quad (3)$$

The equation includes the constants x_1 to x_5. The necessary horsepower is indicated by W_{hp}, while the total head, measured in feet, is symbolized by 'H'.

The energy required to operate the pump must be greater than the W_{hp}. The brake horsepower (BHP), as defined in equation (4), refers to the amount of horsepower required at the pump's shaft to achieve a designated flow rate while overcoming a specific head H.

$$BHP = \frac{W_{hp}}{\text{efficincy of (drive} \times \text{pump)}} \quad (4)$$

Considering Qmax to be 150 gal/minute, H to be 50 meters, and unit pump efficiency, along with a drive efficiency of 0.94, the necessary maximum BHP can be determined by using equation (4), resulting in a value of 4876 watts. The selection of the solar panel's maximum power rating is determined to be 9.6 kW for two motors operating under peak load, based on the maximum BHP. According to equation (2), the motor's maximum speed is calculated to be 190 rad/s, which is roughly equivalent to 1800 rpm. Given a

minimum irradiance level of 200 W/m2, the expected power output of the solar panel will be around 1900 W. Based on the minimum power output of the PV, the SRM will operate at a minimum speed of 720 revolutions per minute.

The load torque acting on SRM(s) is estimated to be TL = 25.0Nm, derived from the maximum speed and power specifications. As water is extracted from underground and brought to the surface, the load torque will rise progressively to T_L from T_b, reflecting the growing weight of the water on the SRM. At the outset, the load torque will be minimal and will progressively rise in a ramp-like manner as the water is released to the target point. When the water arrives at target location, the load torque will remain unchanged. Furthermore, the resistance encountered between the water and the pipe will contribute additional load torque to the motor. Moreover, the incorporation of an extra pipe to deliver water to an alternative target point will result in an increase in load torque. Nevertheless, when both SRMs function concurrently, the load torque will increase twofold.

b. PV System [5, 15-20]

The selection of the PV unit is determined by the power requirements of the two motors discussed in the preceding section. In order to produce the required voltage, a selection of 16 PV modules, each with a power output of 302 watts, has been made. The modules are organized into a PV array, with two such arrays connected in parallel to enhance power generation, yielding a combined output of 2x4800W. For additional details regarding the specifications of the PV modules, kindly consult Table-1.

Table-1: Standard values of PV modules

S.No	Parameter	Value
1	Maximum power of each module.	302
2	Short circuit current.	8.16
3	Open circuit voltage.	48.50
4	PV arrays connected in parallel.	2
5	Voltage at maximum power.	39.60
6	Current at maximum power.	7.66
7	Series modules/array.	16

A total of 32 PV modules were integrated into the WPS, with 16 modules arranged in series to attain the necessary rated power and voltage at DC link. Furthermore, two PV arrays were linked in parallel. Consequently, the probability of the occurrence of PSC rises. Previous studies have conducted a comprehensive modeling of the PSC based PV system in [5, 9]. The voltage associated with the MPP can be monitored through the traditional P&O methodology, which is mathematically defined for consistent solar irradiance.

$$V_{mpp}(t+1) = V_{mpp}(t) + \Delta V \times \text{sign of} \left(\frac{dP_{pv}}{dV_{pv}} \right) \quad (5)$$

This study has examined three distinct PSC patterns, as detailed in Table 2, with the associated voltage versus power curves presented in Figure 2. Figure 2 also displays the MPP along with their associated voltages. In the context of PSC, the PV system may demonstrate several LMPP alongside a single GMPP. Conventional P&O) algorithms possess the ability to identify any of the LMPP. To effectively identify the GMPP, it is essential to utilize a proficient optimization technique. Numerous researchers have investigated optimization methods for PV systems functioning under PSC. For instance, in [14], GA were employed for the purpose of MPPT in PV systems subjected to PSC. Furthermore, a PSO method was devised and introduced in [15]. In a separate investigation, the authors in [5] introduced the MGWO method for PV systems operating under PSC. The POA has attracted considerable interest from researchers owing to its swift convergence rate when compared to conventional methods like GA, PSO, and MGWO. Adding of P&O with the POA presents a viable approach for attaining the MPP in PV systems operating under PSC.

Table-2: Configuration of PSCs

Patterns	Irradiance level of modules in each array
PSC-1	PV Panels: 1-3: 1000 W/m^2, 4-9: 930 W/m^2, 10-12: 800 W/m^2, 13-16: 710 W/m^2.
PSC-2	PV Panels: 1-4: 990 W/m^2, 5-7: 920 W/m^2, 8-13: 780 W/m^2, 14-16: 590 W/m^2.
PSC-3	PV Panels: 1: 820 W/m^2, 2-3: 730 W/m^2, 4-11: 520 W/m^2, 12-16: 350 W/m^2. 0

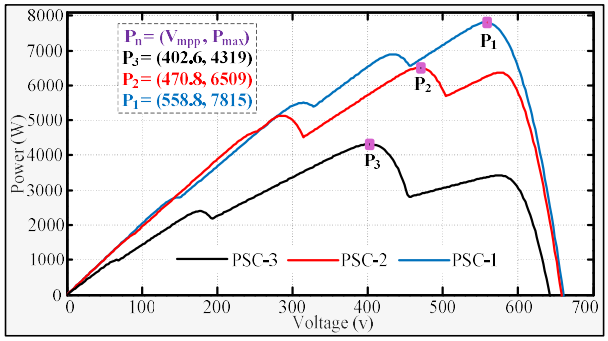

Figure 2: P-V curves as per Table-2.

c. Dynamics of extra pipe.

The incorporation of an extra pipe at the pump outlet is essential for the effective transfer of water between different locations. This procedure will lead to an elevation in both the load torque exerted on the SRM and the pressure head of the pipe, as defined by particular equations. The Hazen Williams formula can be utilized to calculate the head losses.

$$h_l = 0.002083 \times L \times \left(\frac{Q^{1.85}}{d^{4.8655}} \right) \times \left(\frac{100}{C} \right)^{1.85} \quad (6)$$

Similarly, the energy loss resulting from the additional piping can be expressed as.

$$\frac{p_a}{\gamma} + \frac{v_1^2}{2g} + Q_{in} = \frac{p_b}{\gamma} + \frac{v_2^2}{2g} + Q_{out} + h_l \quad (7)$$

If the pipe is horizontal: $Q_{in} = Q_{out}$and $v_1=v_2$.

Hence,

$$h_l = \frac{(p_a - p_b)}{\gamma} \quad (8)$$

The head loss resulting from the flow resistance of water, denoted as h_l, is influenced by the length of the additional pipe 'L', the diameter of the pipe 'd', and the friction coefficient 'C'. The pressures at the inlet and outlet of the extra pipe during the water flow are represented as P_a and P_b, respectively. The initial and final velocities of water within the pipe are denoted as v_1 and v_2, respectively. Gravitational acceleration is represented by the symbol 'g', whereas the density of water is denoted as 'γ'.

III. POPO System Algorithm

The POA is an innovative bio-inspired metaheuristic algorithm that is based on the natural behaviors exhibited by Pufferfish [11]. This paper seeks to illustrate the application of POA and to showcase its efficacy in improving the MPPT algorithm utilized in PV systems. The design of the POA draws inspiration from the distinctive behavior of Pufferfish, which expand their bodies as a means of defense when they feel threatened. In a comparable manner, the POA utilizes a dynamic inflation mechanism to efficiently navigate the search space. The algorithm commences with a foundational group of Pufferfish individuals, each symbolizing a possible solution. These individuals experience multiple iterations, during which they expand or contract in accordance with their fitness values. The inflation mechanism enables Pufferfish individuals to investigate potentially advantageous areas within the search space, whereas deflation facilitates their ability to capitalize on local optima. Through the dynamic alteration of their size, Pufferfish individuals are able to achieve an effective balance between exploration and exploitation, resulting in enhanced convergence speed and accuracy. Figure 3 depicts the Pufferfish in a state of defense. The fundamental idea of POA is inspired by the defensive strategy utilized by Pufferfish to protect themselves from predators. The Pufferfish employs a defensive mechanism by inflating its flexible stomach with water, thereby becoming a round entity covered in sharp spines. As a result, the possible threat is discouraged, thereby facilitating its avoidance of this dangerous circumstance.

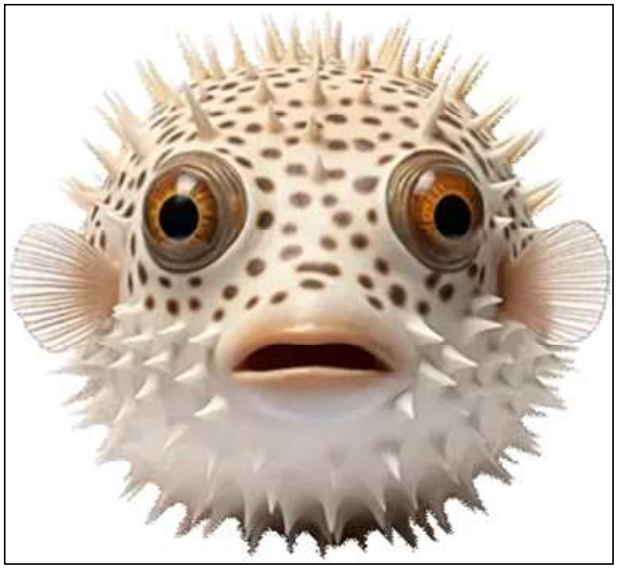

Figure 3: Defensive mode of Pufferfish.

In order to assess the effectiveness of the proposed POA associated MPPT methodology, we carried out comprehensive simulations and made comparisons with several existing algorithms. The findings indicate that the POA surpasses the current algorithms regarding convergence speed, accuracy, and robustness. It consistently demonstrates superior power extraction efficiency and shows enhanced adaptability to diverse environmental conditions. The suggested algorithm demonstrates significant promise in enhancing both the efficiency and reliability of PV systems. The subsequent procedure is executed to establish the POA mechanism for the MPPT of the PV unit.

The vectors present in the community can be expressed mathematically through a matrix, as outlined in Equation (9). The starting position of each member of the POA is determined by Equation (10) at the commencement of the algorithm. Where F is represents voltage point.

$$F=\begin{bmatrix} F_{1,l} & \cdots & F_{1,d} & \cdots & F_{1,m} \\ \vdots & & \vdots & & \vdots \\ F_{i,l} & \cdots & F_{i,d} & \cdots & F_{i,m} \\ \vdots & & \vdots & & \vdots \\ F_{n,l} & \cdots & F_{n,d} & \cdots & F_{n,m} \end{bmatrix} \tag{9}$$

$$F_{i,d}=v_{lb}+r\cdot\left(v_{ub}-v_{lb}\right) \tag{10}$$

$$P_{\max}=\begin{bmatrix} P(F_1) \\ \vdots \\ P(F_i) \\ \vdots \\ P(F_n) \end{bmatrix} \tag{11}$$

Phase-A: Examination of Predator Assault on Pufferfish (Investigation Stage).

In the preliminary phase (Phase-A) of the POA, the positions of the population members are reassessed by employing a simulation of the predator attack strategy aimed at the Pufferfish, which can be expressed by (12).

$$F_{i,j}^{P1}=F_{i,j}+r_{i,j}\cdot\left(SF_{i,j}-L_{i,j}\cdot F_{i,j}\right) \tag{12}$$

Phase 2: The Defensive Strategy of Pufferfish against Predators (Exploitation Phase).

During this phase of the Plan of Action, the positioning of individuals within the population is reassessed by modeling the defensive tactics employed by a Pufferfish in response to predator attacks, as indicated by the expression below.

$$F_{i,j}^{P2}=F_{i,j}+1-2r_{i,j}\cdot\frac{v_{ub}-v_{lb}}{t} \tag{13}$$

In this context, V is the population matrix and P is the vector for the assessed objective function. The random number is denoted as r, while v_{ub} and v_{lb} signify the upper and lower voltage limits of the PV system, respectively. $F_{i,j}^{P1,2}$ represents the updated arrangement of voltages in relation to their respective phases. The term SFi,j denotes the chosen Pufferfish.

The implementation of the TS-Fuzzy controller utilizes mathematical expressions to define the membership functions for the voltage error (V_i) and its derivative ($\dot{V}_i$) signals, which can be categorized into positive (P) and negative (N) values.

The TS-Fuzzy controller employs mathematical formulations to establish the membership functions for the voltage error (V_i) and its derivatives ($\dot{V}_i$), applicable to both positive (P) and negative (N) scenarios.

$$\mu_P(V_i)=\begin{cases}0, & V_i < L_1\\ \dfrac{V_i+L_1}{2L_1}, & -L_1 \le V_i \le L_1 \text{ and}\\ 1, & V_i > L_1\end{cases}$$

$$\mu_N(V_i)=\begin{cases}1, & V_i < L_1\\ \dfrac{-V_i+L_1}{2L_1}, & -L_1 \le V_i \le L_1\\ 0, & V_i > L_1\end{cases} \quad (14)$$

$$\mu_P(\dot{V}_i)=\begin{cases}0, & \dot{V}_i < L_2\\ \dfrac{\dot{V}_i+L_2}{2L_2}, & -L_2 \le \dot{V}_i \le L_2 \text{ and}\\ 1, & \dot{V}_i > L_2\end{cases}$$

$$\mu_N(\dot{V}_i)=\begin{cases}1, & \dot{V}_i < L_2\\ \dfrac{-\dot{V}_i+L_2}{2L_2}, & -L_2 \le \dot{V}_i \le L_2\\ 0, & \dot{V}_i > L_2\end{cases} \quad (15)$$

Table-3: The TS-fuzzy controller rules:

Rules	V_i(k)	$\dot{V}_i$(k)	Values
Rule-A	*N*	*N*	$Z_1 = d_1 V_i(k) + d_2 \dot{V}_i(k)$
Rule-B	*N*	*P*	$Z_2 = d_3 \times Z_1$
Rule-C	*P*	*N*	$Z_3 = d_4 \times Z_1$
Rule-D	*P*	*P*	$Z_4 = d_5 \times Z_1$

The regulations pertaining to the TS-Fuzzy controller are detailed in Table-3. It is crucial to modify the parameters employed in TS-Fuzzy, while the rules $Z_{1to\ 4}$ denote the outcomes of the T-S Fuzzy controller, with k signifying the sampling instant. The fuzzy constants d_{1to5} require precise adjustment. The output value of the TS-Fuzzy (Y) is established through the use of a generalized defuzzifier, by (16).

$$Y = \frac{Z_1 \times B_1 + Z_2 \times B_2 + Z_3 \times B_3 + Z_4 \times B_4}{Z_1 + Z_2 + Z_3 + Z_4} \quad (16)$$

IV. Proposed Controller

In various settings, the extraction of water requires the operation of two or more motors. In these situations, it is crucial to have a multi-motor system operated by a converter, along with an appropriate energy management system and control methodology. The control methodology that demonstrates efficacy for the WPS, as illustrated in Figure 1, is shown in Figure 4. The suggested control method consists of three main components: sensorless speed estimation, the dc-link voltage controller (DCLC), and DTC for the SRM, as depicted in Figure 4. The voltage associated with maximum power is obtained through the hybrid POPO method. The reference speed signal (N_{ref}) for the SMCs is produced by a SMC that evaluates this voltage signal in relation to V_{PV}. The comprehensive internal block diagram of the SMC is illustrated in Figure 5 and modeled by using below equations.

$$\psi_d = (A - B - C + D) \times \cos(\pi/4) \quad (17)$$

$$\psi_q = (A + B - C - D) \times \sin(\pi/4) \quad (18)$$

The determination to activate or deactivate the connection of SRM-2 to the converter is based on the power output produced by the PV system. The switch is designed to engage when the PV power attains 4800 W and will automatically deactivate when the power falls to 1900 W, thereby ensuring that two motors do not operate below the critical speed of 720 RPM. This configuration assists in preventing the occurrence of frequent ON and OFF cycles at designated power levels. When a specific value is established as the limit, the switch will function reliably at that designated level.

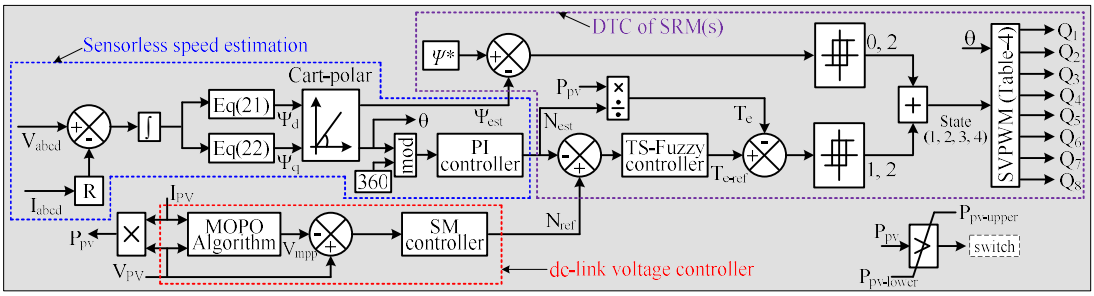

Figure 4: Proposed controller.

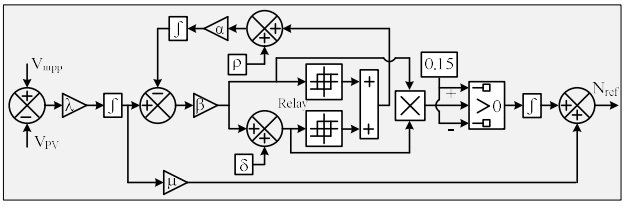

Figure 5: SMC block diagram.

V. Results and Discussions

The controllers developed in this research were executed on a real-time simulator (RTS), and the findings were showcased on the OPAL-RT platform. The RTS effectively replicates the behavior of the PV-based WPS that utilizes SRM, incorporating the suggested control mechanism. Additional details regarding the RTS are available in reference [9]. To establish the Hardware-In-Loop (HIL) configuration, two OPAL-RT units, were employed in conjunction with their computer system. One unit was designated for the operation of the WPS in conjunction with the PV, converter, SRMs, and pumps, as illustrated in Figure 1, whereas the other unit was allocated for the implementation of the controllers associated with this model. The configuration involving HIL with OPAL RT devices is illustrated in Figure 6.

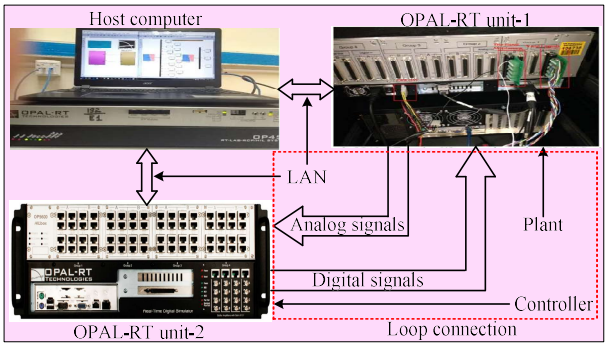

Figure 6: Configuration of HIL.

The WPS dynamic unit (OPAL RT1) transmits analogue signals to the control unit (OPAL RT2), whereas the digital signals are relayed from the controller unit to the WPS unit. The OPAL-RT units communicate via genuine digital and analog signals, establishing a HIL connection between OPAL-RT-1 and OPAL-RT-2, which facilitates the effective monitoring of real-time dynamics. Figure 7 illustrates the comprehensive block diagram of the HIL system, which incorporates two OPAL-RT units.

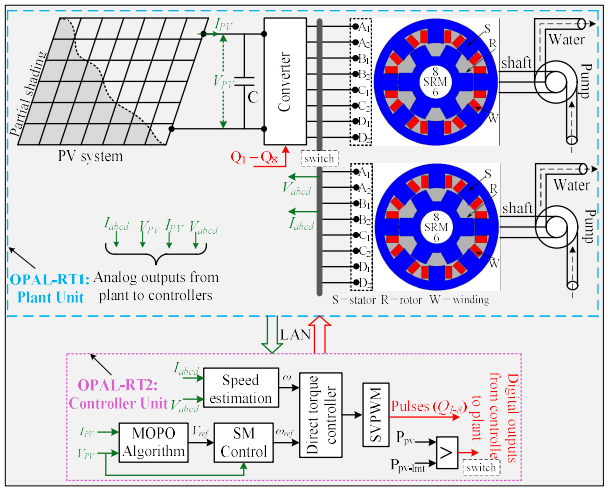

Figure 7: HIL implementation of WPS.

Case-1: Response of PV under PI and SMC.

In this situation, a variation in solar irradiance from 1000 to 750W/m² is being examined at t = 3.0 seconds. The assessment of DCLC's performance is conducted through the application of both PI and SMC, as demonstrated in Figure 5. The optimization of the PI gains is tailored for an irradiance level of 1000 W/m2; however, their performance diminishes when the irradiance decreases to 750 W/m2. Conversely, the SMC exhibits the ability to modify the output in reaction to variations in irradiance. Figure 8 illustrates the reference and actual powers produced by the PV system utilizing both PI and SMCs. Figure 8 shows that the MPPT performance is improved with the SMC compared to the PI controller, highlighting the value of SMC in optimizing power extraction from PV systems in Direct DCDC converters. Furthermore, the absence of adjustment of the PI gains for an irradiance level of 750 W/m2 leads to heightened oscillations in the voltage at dc-link, which adversely affects the capacity to optimize power extraction from the PV unit. As a result, additional research is carried out utilizing the SMC-based DCLC.

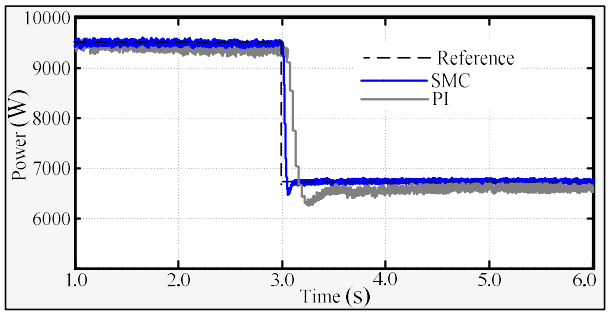

Figure 8: Powers.

Case-2: Performance among various optimizations.

The main challenge involves enhancing power output in PV systems under PSC. A new hybrid POPO algorithm has been created and evaluated in comparison to PSO, GA, and MGWO algorithms, each of which has been integrated with the P&O mechanism for different PSC scenarios as detailed in Table-2. The PV characteristics for the various PSC scenarios are depicted in Figure 2, whereas the associated comparisons of power generation are presented in Figure 9. This research assumes a constant irradiance level until t=3 seconds, after which PSC-1 is introduced from t=3 to t=5 seconds, PSC-2 from t=5 to t=7 seconds, and PSC-3 from t=7 to t=9 seconds. The examination of Fig. 9 indicates that the hybrid POPO algorithm demonstrates superior performance compared to GA, PSO, and MGWO in optimizing power output from the PV system during the designated tracking period. Consequently, the suggested hybrid POPO algorithm facilitates a more effective energy harvesting process from the PV unit. Furthermore, Figure 10 illustrates the associated voltages under PSCs in conjunction with the POPO algorithm.

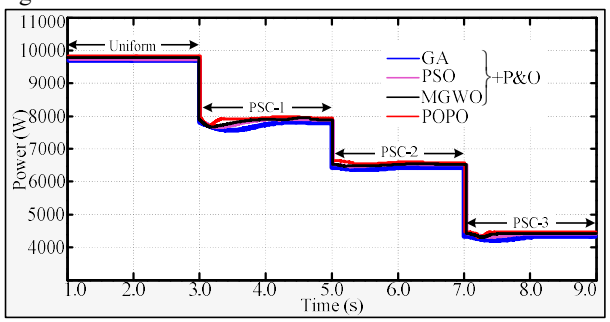

Figure 9: Various powers.

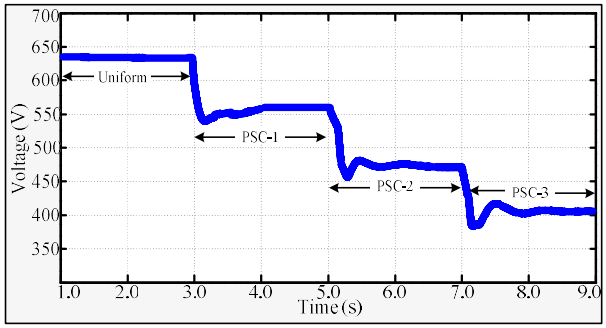

Figure 10: Voltage with POPO.

The bar chart presented in Figure 11 depicts the comparisons for tracking responses of the PV unit under PSCs. The suggested hybrid POPO algorithm demonstrates considerable advantages and exhibits superior performance

during PSC when compared to PSO, GA, and MGWO. This is attributed to its capacity to rapidly monitor V_{mpp} in comparison to alternative optimization methods.

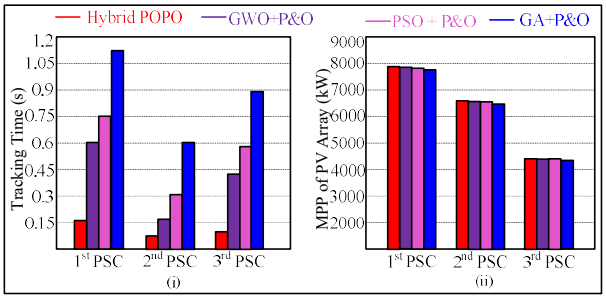

Figure 11: Comparisons.

Case-3: Under the operation of two SRMs.

Under low irradiance conditions, the power produced by the PV unit is adequate to operate solely one SRM. Generally, the PV system generates reduced energy output during the morning and evening hours, as well as in conditions of significant partial shading. In these situations, only a single SRM is employed. When the power attains its maximum threshold (P_{PV}-upper as illustrated in Figure 4), the second SRM is automatically linked to the converter via a switch. This connection can be established when there is an increase in irradiance. Consequently, the velocity of the initial SRM promptly diminishes as a result of the power distribution between the two SRMs. The initial solar irradiance is established at 450 W/m²; however, it experiences a sudden increase to 650 W/m² at t = 1.5 seconds to facilitate the functioning of both SRMs, as illustrated in Figure 12. As a result, the PV power begins to rise, which in turn causes acceleration in the speed of SRM-1. When the power produced by the PV unit attains its maximum threshold (P_{PV}-upper), the switch automatically links SRM-2 to the identical converter. This connection takes place around t=1.68 seconds, resulting in a gradual reduction in the speed of SRM-1, while the speed of SRM-2 experiences a gradual increase. Both engines achieve stability at approximately 1200 RPM. The reference speed of the SRM is also reduced as a result of the abrupt drop in DC-link voltage triggered by the sudden engagement of SRM-2. At t=2.25 seconds, the irradiance rises to 1000 W/m². The velocities of both motors rise uniformly and attain a stable condition at approximately t=2.5 seconds. The detailed illustration of how the speed of the SRMs varies with changes in solar irradiance is presented in Figure 12. The upper line of the PPV indicates the threshold for the functioning of either one or two SRMs. The left portion of the line illustrates the functioning of a single SRM, whereas the right portion demonstrates the operation of both SRMs.

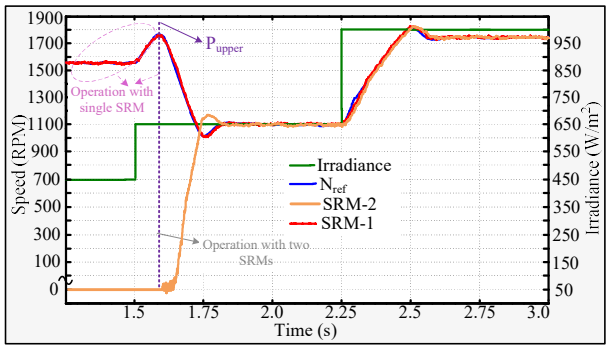

Figure 12: Working under both motors.

Case-4: Working with an extra pipe

In WPSs, it is customary to incorporate an additional pipe to facilitate the transfer of water from one location to another. Generally, pipes made of PVC, HDPE, Lateral, and LDPE are employed for this application. The torque increases as the length of the pipe extends due to the friction and external forces exerted on the water within the pipe.

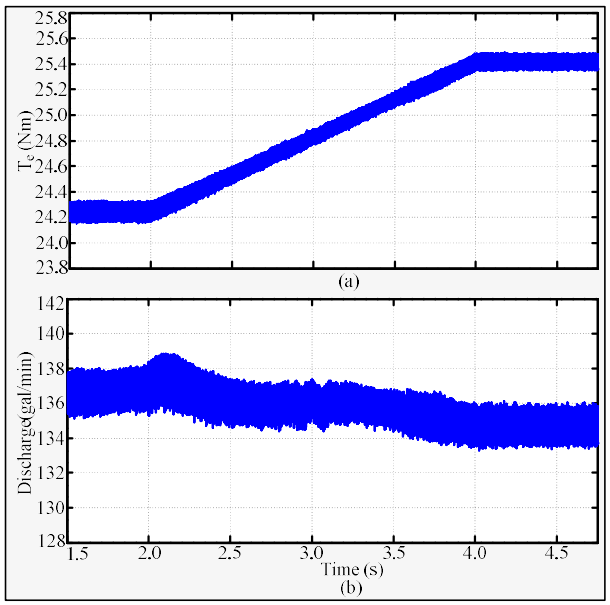

Figure 13: responses of (a) torque (b) discharge.

Furthermore, the torque exerted on the motor progressively increases until the water flows to the new outlet following the installation of an additional pipe in the bore well. In this scenario, a pipe length of 20 meters is considered for the transportation of water from the bore well outlet to the designated location, with the associated torque and water discharge illustrated in Figures 13 (a) and (b) respectively. As the torque applied to the motor rises, the speed of the motor diminishes, although the power output stays unchanged. As a result, the water flow remains consistent when the pipe is aligned horizontally with the ground. Nevertheless, there could be a minor reduction in water discharge attributed to losses resulting from friction and external forces that oppose the motor's power and torque.

VI. CONCLUSIONS

The PSC of the PV fed WPS, which is powered by SSC SRMs, employs the hybrid POPO algorithm, facilitated by

the integration of SMC and DTC. To assess the tracking behavior of the MPPT under PSCs in a PV unit, the proposed method is compared with PSO, GA, and MGWO. The findings are displayed for various practical scenarios utilizing the OPAL-RT platform. In order to attain a rapid response in tracking the voltage at dc-link, the SMC-based DCLC has been implemented. It has been noted that the implementation of SMC demonstrates a considerable capacity to modify the output in alignment with the MPP when compared to the PI. The model highlights the need to choose WPS within PSC, while addressing practical challenges like installing extra pipes for water transport and considering load torque on SRM. Comprehensive results are presented to substantiate the proposed method on the OPAL-RT platform. The proposed hybrid POPO algorithm has been found to facilitate the extraction of greater energy from the PV system. The suggested model aims to be economically efficient, eliminating the requirement for energy storage solutions such as batteries or additional DC circuits for the MPPT of the PV unit. Efficient controllers are engineered to accommodate a range of potential operations involving two motor-pump assemblies.

References

[1]. S. G. Malla, "Small signal model of PV power generation system," 2017 IEEE International Conference on Power, Control, Signals and Instrumentation Engineering (ICPCSI), Chennai, India, 2017, pp. 3069-3073, doi: 10.1109/ICPCSI.2017.8392289.

[2]. Malla, Siva Ganesh, Malla, Jagan Mohana Rao, Malla, Priyanka, Ramasamy, Sreekanth, Doniparthi, Satish Kumar, Sahu, Manoj Kumar, Subudhi, Pravat Kumar and Awad, Hilmy. "Coordinated power management and control of renewable energy sources based smart grid" *International Journal of Emerging Electric Power Systems*, vol. 23, no. 2, 2022, pp. 261-276. https://doi.org/10.1515/ijeeps-2021-0113

[3]. T. Anuradha et al., "Power Quality Improvement of Hybrid Standalone Microgrid with DSTATCOM during Faults on Distribution Line," 2022 IEEE International Conference on Power Electronics, Drives and Energy Systems (PEDES), Jaipur, India, 2022, pp. 1-7, doi: 10.1109/PEDES56012.2022.10080027.

[4]. D. Vannurappa, G. P. R. Reddy, K. Deepak, Y. Hazarathaiah, S. S. Prasad and S. G. Malla, "Small Signal Analysis of Photovoltaic based Water-Pumping System Driven by Induction Motor," 2023 7th International Conference on Computing Methodologies and Communication (ICCMC), Erode, India, 2023, pp. 15-20, doi: 10.1109/ICCMC56507.2023.10083929.

[5]. P. Bellamkonda et al., "Modified Grey Wolf Optimization Algorithm for PV Fed Water Pumping System Driven by Switched Reluctance Motor under Partial Shading Condition," 2022 IEEE International Conference on Power Electronics, Drives and Energy Systems (PEDES), Jaipur, India, 2022, pp. 1-6, doi: 10.1109/PEDES56012.2022.10080719.

[6]. Malla, S.G., Malla, P., Karthik, M. *et al.* Modified Invasive Weed Optimization for the Control of Photovoltaic Powered Induction Motor Drives in Water Pumping Systems. *Iran J Sci Technol Trans Electr Eng* **47**, 925–938 (2023). https://doi.org/10.1007/s40998-023-00589-7.

[7]. V M Revathi and K Subramani and S Krishnakumar and Ahmed Hussein Alawadi and R Senthil Kumar and Siva Ganesh Malla, "A modified invasive weed optimization for MPPT of PV based water pumping system driven by induction motor", IOP: Engineering Research Express, volume 6, number 3, July 2024, https://dx.doi.org/10.1088/2631-8695/ad5cd3.

[8]. Kandi Bhanu Prakash, "Modeling of DC to DC Converter for Renewable Energy Sources", International Journal of New Technologies in Science and Engineering (IJNTSE), Vol. 9, Issue. 1, pp. 6-10, Jan. 2023.

[9]. S. G. Malla et al., "Whale Optimization Algorithm for PV Based Water Pumping System Driven by BLDC Motor Using Sliding Mode Controller," in IEEE Journal of Emerging and Selected Topics in Power Electronics, vol. 10, no. 4, pp. 4832-4844, Aug. 2022, doi: 10.1109/JESTPE.2022.3150008.

[10]. M. B. Lakshmi et al., "Voltage and Frequency Control of a PV-Battery-Diesel Generator based Standalone Hybrid System," 2022 IEEE International Conference on Power Electronics, Drives and Energy Systems (PEDES), Jaipur, India, 2022, pp. 1-7, doi: 10.1109/PEDES56012.2022.10080764.

[11]. Al-Baik, O.; Alomari, S.; Alssayed, O.; Gochhait, S.; Leonova, I.; Dutta, U.; Malik, O.P.; Montazeri, Z.; Dehghani, M. Pufferfish Optimization Algorithm: A New Bio-Inspired Metaheuristic Algorithm for Solving Optimization Problems. Biomimetics 2024, 9, 65. https://doi.org/10.3390/biomimetics9020065.

[12]. M. Muddhey, R. K. Behera and U. R. Muduli, "Solar PV and Battery Assisted Isolated Power Supply Control and Implementation," 2022 IEEE International Conference on Power Electronics, Drives and Energy Systems (PEDES), Jaipur, India, 2022, pp. 1-5, doi: 10.1109/PEDES56012.2022.10080581.

[13]. S. Prakash, O. A. Zaabi, R. K. Behera, K. A. Jaafari, K. A. Hosani and U. R. Muduli, "Modeling and Dynamic Stability Analysis of the Grid-Following Inverter Integrated With Photovoltaics," in IEEE Journal of Emerging and Selected Topics in Power Electronics, vol. 11, no. 4, pp. 3788-3802, Aug. 2023, doi: 10.1109/JESTPE.2023.3272822.

[14]. D. Fares, M. Fathi and S. Mekhilef, "Comparison of Two Hybrid Global Maximum Power Point Algorithms for Photovoltaic Module Under Both Uniform and Partial Shading Condition," 2020 International Conference on Electrical, Communication, and Computer Engineering (ICECCE), Istanbul, Turkey, 2020, pp. 1-6, doi: 10.1109/ICECCE49384.2020.9179426.

[15]. R. Sangrody, S. Taheri, A. -M. Cretu and E. Pouresmaeil, "An Improved PSO-Based MPPT Technique Using Stability and Steady State Analyses Under Partial Shading Conditions," in IEEE Transactions on Sustainable Energy, vol. 15, no. 1, pp. 136-145, Jan. 2024, doi: 10.1109/TSTE.2023.3274939.

[16]. Mansour Aljohani, Siva Ganesh Malla and Mohamed I. Mosaad, TS-Fuzzy Controllers based Novel Control of Grid Connected Fuel Cell Stack System, E3S Web of Conf., Volume 540, 2024, https://doi.org/10.1051/e3sconf/202454010005.

[17]. S. K. Baksi, R. K. Behera and U. R. Muduli, "A new Transformerless Five-level Boost Inverter with Minimum Switch Count For Photovoltaic Application," 2023 IEEE 3rd International Conference on Smart Technologies for Power, Energy and Control (STPEC), Bhubaneswar, India, 2023, pp. 1-6, doi: 10.1109/STPEC59253.2023.10430976.

[18]. S. K. Baksi, R. K. Behera and U. R. Muduli, "Comprehensive Overview of Reduced Switch Count Multilevel Inverter for PV Applications," 2023 IEEE 3rd International Conference on Smart Technologies for Power, Energy and Control (STPEC), Bhubaneswar, India, 2023, pp. 1-6, doi: 10.1109/STPEC59253.2023.10431075.

[19]. J. K. Singh et al., "Active Disturbance Rejection Control of Photovoltaic Three-Phase Grid Following Inverters Under Uncertainty and Grid Voltage Variations," in IEEE Transactions on Power Delivery, vol. 38, no. 5, pp. 3155-3168, Oct. 2023, doi: 10.1109/TPWRD.2023.3266898.

[20]. S. K. Baksi, R. K. Behera and U. R. Muduli, "Optimized 9-Level Switched-Capacitor Inverter for Grid-Connected Photovoltaic Systems," in IEEE Transactions on Industry Applications, vol. 60, no. 2, pp. 3284-3296, March-April 2024, doi: 10.1109/TIA.2023.3332059.